

Flipping magnetization induced by noncollinear ferromagnetic-antiferromagnetic exchange coupling

B. Y. Wang,¹ C. H. Chuang,¹ S. S. Wong,¹ J. J. Chiou,² W. C. Lin,² Y. L. Chan,³ D. H. Wei,³ and Minn-Tsong Lin^{1,4,*}

¹*Department of Physics, National Taiwan University, Taipei 106, Taiwan*

²*Department of Physics, National Taiwan Normal University, Taipei 116, Taiwan*

³*National Synchrotron Radiation Research Center, Hsinchu 300, Taiwan*

⁴*Institute of Atomic and Molecular Sciences, Academia Sinica, Taipei 106, Taiwan*

(Received 3 November 2011; published 7 March 2012)

We present a direct observation of a flipping magnetization of a uniform Fe film/wedged-Mn bilayer induced by a biquadratic-type exchange coupling established at the interface. The element-resolved magnetic imaging shows that the Fe film exhibited a flipping of magnetization between the $[\bar{1}00]$ and $[010]$ directions with a periodicity of one monolayer Mn thickness as below a critical temperature. The enhancement of the variation angle with the increase of Mn thickness follows the tendency of the finite-size effect of antiferromagnetism on interface exchange coupling. The flipping magnetization emerging coincidentally with the uncompensated-compensated transition of Mn magnetic surface indicates a frustration-induced biquadratic-type interface exchange coupling, and suggests a layered-like uncompensated AFM ordering for the Mn layer.

DOI: [10.1103/PhysRevB.85.094412](https://doi.org/10.1103/PhysRevB.85.094412)

PACS number(s): 75.50.Ee, 75.60.-d, 75.70.Kw, 75.70.Rf

I. INTRODUCTION

The exchange coupling across the interface of antiferromagnetic (AFM)/ferromagnetic (FM) bilayers results in characteristic phenomena, namely exchange bias and coercivity enhancement.¹ The great impact has been undoubtedly proved by its important applications on magnetic storage devices.^{2,3} To date, researchers have reported that the exchange coupling between FM and AFM spins could occur in either a collinear or noncollinear way, depending on the interface spin arrangements of the AFM layer. For an AFM/FM bilayer with a fully uncompensated AFM order and a smooth interface, the collinear (either parallel or antiparallel) type of coupling could be the stable state, which may force the FM spins in line with the AFM spins when the coupling is established.^{1,4} For the bilayer with the AFM film having intrinsically compensated spin order at each layer⁵ or the rough interface⁶ which causes spin frustration at the surface of the antiferromagnet, the noncollinear (spin-flop) coupling could be established to minimize the interface exchange energy.⁷⁻⁹

It has been suggested that the noncollinear type of exchange coupling at an interface could also induce a flipping of the FM spins in the FM/AFM bilayer, in which the direction depends on the sum of spin vectors at the AFM surface.^{10,11} This may provide an alternative way to explore the AFM spin structure, which is intriguing from both scientific and application aspects. However, although the flipping phenomenon of FM spins has been reported in many FM/AFM systems,¹²⁻²² the mapping of the AFM spin orientation on individual layers is difficult, because the rotation of FM spins could be induced by the AFM surface spin vectors summed over several adjacent layers determined by the degree of interfacial roughness. Current studies usually compare the observed rotation angle to the theoretically proposed AFM spin structure with the additional symmetry owing to a “rough” interface.¹⁶⁻²² However, a direct comparison of FM spin rotation and interfacial AFM spins on a single-crystalline FM/AFM bilayer with a well-defined AFM-FM interface has not been reported.

Among the metallic antiferromagnets, Mn films are regarded as highly interesting systems due to abundant magnetic phases that are strongly correlated with the crystalline structures.^{23,24} It has been theoretically suggested that the face-centered-cubic (fcc) Mn ($c/a = 1$) behaves with two energetically degenerate magnetic states, namely the in-plane $c(2 \times 2)$ (compensated) and the $[100]$ layered (uncompensated) AFM structures.^{23,24} Since the compensated and uncompensated surface spin structures of the AFM layer were expected to lead to the collinear and noncollinear type of exchange coupling with the adjacent FM layer, respectively, it is possible to distinguish the preferred interfacial spin arrangement of the fcc-Mn layer in the FM/fcc-Mn bilayer by examining the characteristic of induced magnetization flipping of the FM film with the variation of Mn film thickness or temperature.

In this paper, we clarify the correlation between the magnetization flipping of an FM layer and interface exchange coupling by performing an investigation on an ultrathin thin Fe/wedged-Mn bilayer with the technique of element-resolved magnetic imaging in application of x-ray photoemission electron microscopy (PEEM). From the result of an observed 90° flipping magnetization of the Fe layer emerging coincidentally with the uncompensated-compensated transition of the Mn magnetic surface, we identify a frustration-induced collinear to noncollinear transition of interface exchange coupling originating from a layered-like AFM order of the Mn layer.

II. EXPERIMENT

The samples were prepared *in situ* in the UHV multifunctional NTU-NSRRC Nanomagnetism Chamber (base pressure = 2×10^{-10} torr). This chamber was connected with a PEEM end station at beamline BL05B2 of the NSRRC, Taiwan, for magnetic imaging with synchrotron x-rays.^{25,26} The sample of the 8 ML Fe/wedged-Mn bilayer was prepared on a $\text{Cu}_3\text{Au}(001)$ substrate at room temperature (RT), in which the preparation procedures of $\text{Cu}_3\text{Au}(001)$ and the wedged sample are described in Refs. 27 and 28.

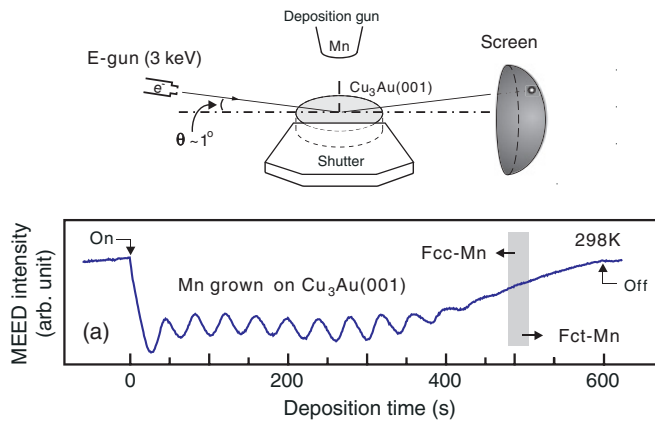


FIG. 1. (Color online) Reflected specular (0, 0) beam intensity for the Mn film grown on $\text{Cu}_3\text{Au}(001)$ as a function of deposition time at RT. The regular oscillation indicates a layer-by-layer growth mode. A fcc-fct structural transition was observed as $t_{\text{Mn}} > 11$ ML (Refs. 27 and 30). The top schematic diagram indicates the illustration of MEED measurement.

The growth of thin films was monitored by medium energy electron diffraction (MEED) (see schematic diagram of Fig. 1). The beam energy was set to 3 keV, and the glancing angle was precisely tuned to a condition of destructive interference between the electron beam and film. For a thin film grown on substrate with layer-by-layer growth mode, the intensity of the reflected specular spot can be modulated with the variation of film thickness. Thus, by monitoring the oscillation of specular spot intensity, an accurate control on the completion of integer or half-integer monolayers can be achieved. Figure 1 shows the recorded MEED reflected specular spot intensity of the Mn film as a function of deposition time. The regular oscillation indicates a well-defined layer-by-layer growth mode, in which the flat surface with around two monoatomic steps has been observed by STM.^{27,29} As $t_{\text{Mn}} > 11$ ML, the oscillation was found to vanish coincidentally with the fcc-fct structural transition as reported in the previous studies.^{27,30}

Experimentally, there are four different phases observed for the bulk Mn. The α phase has a complex cubic structure with 58 atoms per unit cell and noncollinear AFM order which disappears above the Néel temperature of 95 K.³¹ For the temperature above 1073 K, a transition to a cubic structure with 20 atoms per unit cell occurs, namely the β phase.³² For the temperature between 1368 K and 1406 K, the γ phase with fcc structure appears. Finally, there exists another δ phase with bcc structure for the temperature between 1406 K and the melting temperature 1517 K. Since the temperatures leading to the presence of the last three phases could be much higher than their Néel temperatures, the AFM characteristics of them are unlikely to be investigated in bulk form. Alternatively, it has been reported that the fcc-like phases of Mn films can be stabilized at room temperature through an epitaxial growth on $\text{Cu}_3\text{Au}(100)$ ^{27,30} or $\text{Co/Cu}(001)$.^{33,34} A metastable phase of fcc-Mn ($c/a \sim 1$) can be stabilized at $\text{Cu}_3\text{Au}(100)$ for the thickness of Mn film less than ~ 11 ML.^{27,28} For the thicker Mn films, the presence of slight tetragonal distorted fct states (i.e., $c/a \sim 0.96$ and $c/a \sim 1.05$ for the former and latter cases) was suggested to be accompanied by

two antiferromagnetic ground states of in-plane $c(2 \times 2)$ and layered AFM, respectively, as below the bulk Néel temperature of about 540 K.^{30,35,36} Interestingly, as mentioned earlier, the ground-state energies of in-plane $c(2 \times 2)$ and layered-AFM states could become degenerate for a fcc Mn.^{23,24} In such scenario, fcc-Mn film could reveal novel magnetic properties. For example, a perpendicular magnetic anisotropy was found to be established in 6 ML Fe/fcc-Mn bilayers while the thickness of fcc-Mn ultrathin film is thicker than 2 ML and at low temperature.²⁸

In the present work, we focus on the investigation of Fe/fcc-Mn bilayers with only in-plane magnetic anisotropy by choosing the thicker 8 ML Fe layer with the stronger in-plane shape anisotropy. According to previous works,^{37,38} the anisotropy of Fe film was found to be biaxial aligning in in-plane (110) directions [with respect to the fcc- $\text{Cu}_3\text{Au}(001)$ crystalline axis]. The structure of the films was monitored by low energy electron diffraction (LEED) and LEED I/V.²⁸ The observed body-centered-tetragonal (bct) structure of the Fe films is nearly invariant upon varying the Mn underlayer thickness or changing the temperature from 100 K to 300 K.²⁸ Thus, significant structural effects on the magnetic properties of 8 ML Fe/Mn bilayer can be excluded. The magneto-optical Kerr effect (MOKE), assisted by the lock-in technique, was used to measure the hysteresis loops in some selected uniform samples.

Synchrotron radiation x-ray magnetic circular dichroism (XMCD) with PEEM was adopted for element-resolved magnetic domain imaging (Fe and Mn). We focus on imaging with XMCD, because the effect of x-ray magnetic linear dichroism in metallic Mn is very weak due to the vanishing of the crystal-field splitting.⁴ As presented in Fig. 2(a), the magnetism information of individual elements can be obtained from the asymmetry of the XMCD curve at the $L_{3,2}$ absorption edges. Combining XMCD and PEEM, the full-field view of the emitted secondary electrons from the magnetic sample can be resolved by a CCD camera through the use of a multichannel plate. The contrast normalization is achieved by doing imaging calculation on the two full-field images, taken at the Fe (or Mn) L_3 and L_2 edges, respectively, with the formula of $(L_3 - L_2)/(L_3 + L_2)$, based on the fact that normally the XMCD asymmetry is inverted in sign at L_3 and L_2 edges.⁴ As shown in Fig. 2(c), the magnetic contrast can be much enhanced by applying the normalization on the raw images of Figs. 2(d) and 2(e). In the present work, the magnetic imagings were performed at as-grown condition without applying any magnetic field, and first taken at room temperature, and then at 190 K and 105 K.

III. RESULTS

A. Flipping magnetization of Fe film mapped by magnetic domain imaging

Figure 3(a) shows the Fe magnetic image of the 8 ML Fe/wedged-Mn bilayer with the right circularly polarized (RCP) x-rays at RT. The incident x-rays make an angle of 5° from the in-plane $[0\bar{1}0]$ crystallographic direction and 25° from the surface plane, as displayed in the illustration. Two characteristic magnetization directions (i.e., $[\bar{1}10]$ and $[1\bar{1}0]$) were observed for $t_{\text{Mn}} < 8.5$ ML, which agrees with the previous hysteresis-loop measurements on 8 ML Fe/ $\text{Cu}_3\text{Au}(001)$.³⁸

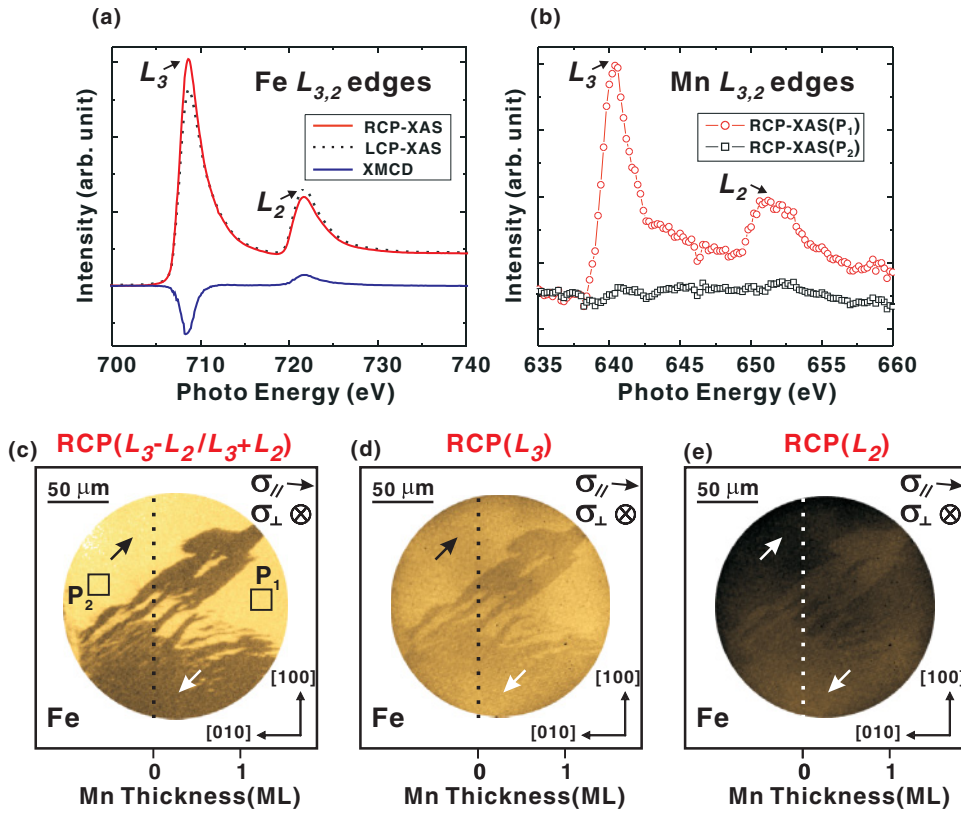


FIG. 2. (Color online) (a) Fe $L_{3,2}$ edge XAS and XMCD spectra of uniform 8 ML Fe film measured by RCP and LCP x-rays at as-grown condition. (b) shows the Mn $L_{3,2}$ edge RCP-XAS spectra averaged over the square areas of P_1 (8 ML Fe/1.2 ML Mn) and P_2 [8 ML Fe/Cu₃Au(001)] in (c). (c) shows the magnetic domain image of 8 ML Fe/wedged-Mn bilayer at the boundary where the t_{Mn} starts to increase from zero value (indicated by the dashed line). A much enhanced magnetic domain contrast is obtained by normalizing the raw images of the L_3 edge (d) and L_2 edge (e) with the formula of $(L_3 - L_2)/(L_3 + L_2)$.

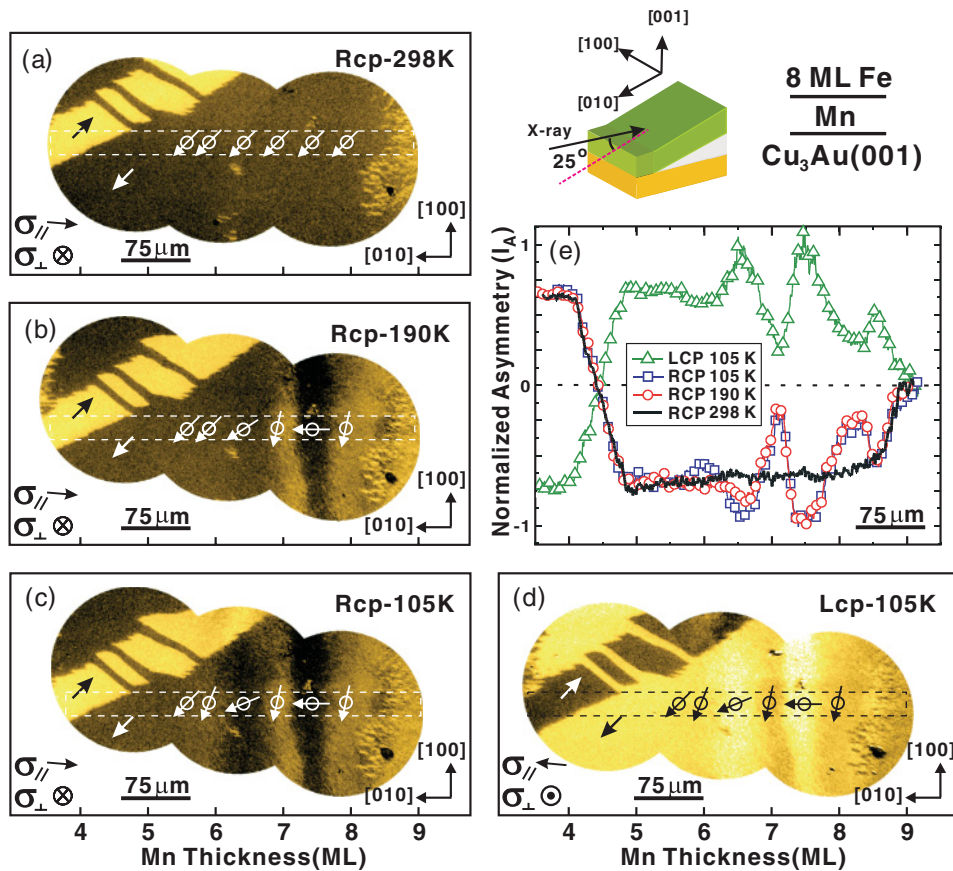


FIG. 3. (Color online) Fe domain images of 8 ML Fe/wedged-Mn/Cu₃Au(001) measured with RCP x-rays at (a) 298 K, (b) 190 K, and (c) 105 K. (d) shows the image at the same position and temperature as (c), but measured by left circularly polarized (LCP) x-rays. (e) shows the normalized XMCD asymmetry (I_A) profiles taken from the average of the region bounded by dashed lines in each domain image.

As $t_{\text{Mn}} \geq 8.5$ ML, the dramatically reduced domain size suggests an obvious exchange coupling effect, which agrees with the behavior reported in FeMn/Co bilayers.²⁰ For the domain revealing a $[\bar{1}10]$ uniform magnetization direction at RT ($t_{\text{Mn}} < 8.5$ ML), the striplike pattern emerges at the lower temperatures [Figs. 3(b) and 3(c)]. In particular, the pattern was extended from the region of the thicker t_{Mn} toward that of the thinner one as the temperature was decreased from 1907nbsp;K to 105 K. By applying x-rays with opposite helicity [Fig. 3(d)], the pattern shows totally inverse contrast. This indicates the Fe film in the region showing a striplike pattern is still ferromagnetic. Since the magnetic contrast of XMCD-PEEM images comes from a projection of magnetization of magnetic domains along the beam direction, the enhanced contrast presenting in the striplike pattern, as compared with that of the preceding $[\bar{1}10]$ domain, indicates the magnetization direction of Fe film in that region should be more parallel to the $[010]$ direction.

By averaging the regions bounded by the dashed lines of Figs. 3(a)–3(d), the normalized magnetic asymmetry (I_A) as a function of t_{Mn} at different temperatures can be obtained, as plotted in Fig. 3(e). With these curves, the magnetization angles of Fe film can be derived according to the XMCD theory: $I_A = \vec{\sigma}_{\parallel} \cdot \vec{M} = \sigma_{\parallel} M \cos \theta$,⁴ where $\vec{\sigma}_{\parallel}$ is the in-plane photohelicity vector which makes a 5° angle to the $[0\bar{1}0]$ direction for a RCP incident x-ray. \vec{M} is the magnetic moment density which has a constant magnitude for a uniform 8 ML Fe overlayer. In the present work, both $\vec{\sigma}_{\parallel}$ and \vec{M} are normalized to unit vectors, in which θ is the included angle. Therefore, the magnetization angle θ with respect to the $[0\bar{1}0]$ direction can be extracted from the I_A of Fig. 3(e) according to above equation. Figure 4(a) shows the θ as a function of t_{Mn} at different temperatures. At RT, $\theta \sim 45^\circ$ corresponds to the $[\bar{1}10]$ magnetization direction as indicated by the arrows of Fig. 3(a). The slight deviation may be attributed to the background variation of the Fe film at different t_{Mn} . As the temperature goes down, θ reveals the tendency to approach 0° ($[010]$ direction) for the Mn layer with half-integer layer thickness, but to 90° ($[\bar{1}00]$ direction) for that with integer layer thickness, presenting a behavior of $\sim 90^\circ$ flipping magnetization with the periodicity of 1 ML Mn thickness.

B. Flipping magnetization of Fe film modulated by finite-size effect of antiferromagnet

We emphasize that the Fe magnetization starts to reorient as the t_{Mn} goes beyond a threshold value. As indicated by the arrows of Fig. 4(a), the threshold thickness is shifted from the lower thickness (t_{c1}) to the higher thickness (t_{c2}), as the measurement temperature is elevated from 105 K to 190 K. This tendency can be simply explained if the AFM-FM exchange coupling is considered as the origin. According to the finite-size effect^{39,40} on low-dimensional magnetic material, the magnetic ordering temperature (T_{ordering}) of an ultrathin AFM film could increase as the AFM film thickness gets thicker, and finally saturate to the bulk value. In the present case, the T_{ordering} of the Mn layer can also increase as the t_{Mn} gets thicker. Once the t_{Mn} is thicker than a threshold thickness, the sufficiently high T_{ordering} of the Mn layer allows Mn-Fe exchange coupling to be established, which leads to

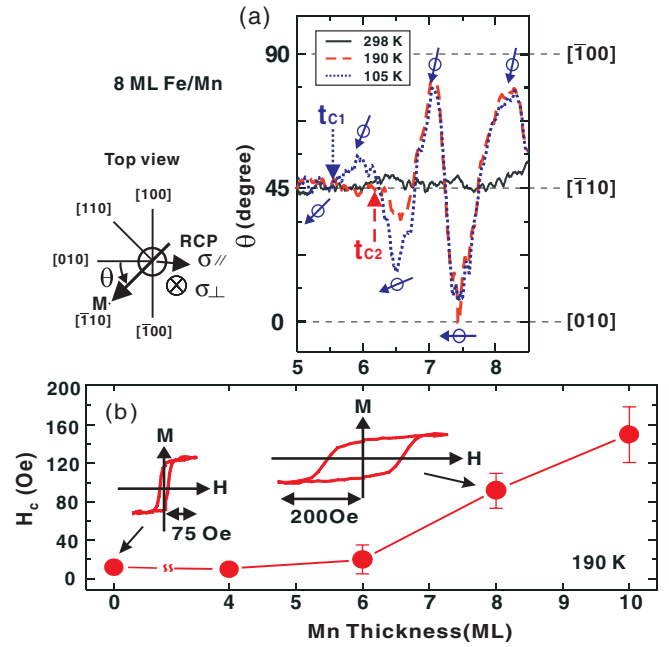


FIG. 4. (Color online) (a) The magnetization direction angle θ of 8 ML Fe film as a function of t_{Mn} at 298 K, 190 K, and 105 K with RCP incident x-rays. At low temperatures, the magnetization direction of the Fe film starts to reorient as the t_{Mn} are thicker than the threshold thicknesses (indicated by t_{c1} and t_{c2} for 105 K and 190 K, respectively) and then prefers to align in the $[010]$ direction for the Mn layer with half-integer layer thickness, but in the $[\bar{1}00]$ direction for Mn layer with integer layer thickness. (b) The coercivity (H_c) of 8 ML Fe/Mn bilayers with the variation of t_{Mn} , measured at 190 K.

the 90° flipping magnetization behavior of Fe film. As the measurement temperature is elevated from 105 K to 190 K, the threshold thickness shifting to the higher coverage (t_{c1} to t_{c2}) is simply due to the requirement of the higher T_{ordering} for establishing the Mn-Fe exchange coupling. Our interpretation of an origin in AFM-FM exchange coupling is also supported by the hysteresis loop measurement. Comparing Fig. 4(a) with Fig. 4(b), the threshold thickness of the flipping magnetization at 190 K (t_{c2}) is very close to the critical thickness of the coercivity enhancement of the uniform 8 ML Fe/Mn bilayers (~ 6 ML) at the same temperature. This further confirms the simultaneously existing Mn-Fe exchange coupling and flipping magnetization, because the phenomenon of coercivity enhancement is well accepted to be a fingerprint of the AFM-FM exchange coupling.¹

C. Noncollinear-type exchange coupling between Fe and Mn layers

A deeper understanding of the Mn-Fe exchange coupling can be achieved by applying the magnetic domain imaging on the Mn element. Figure 5 shows the Fe and Mn domain images, and corresponding magnetic asymmetry I_A curves, at 105 K. Despite the magnetic asymmetry of the Mn domain being very weak, which might be due to a nearly orthogonal included angle between the beam direction and in-plane magnetization of the Mn layer, we can still recognize that the larger magnetic

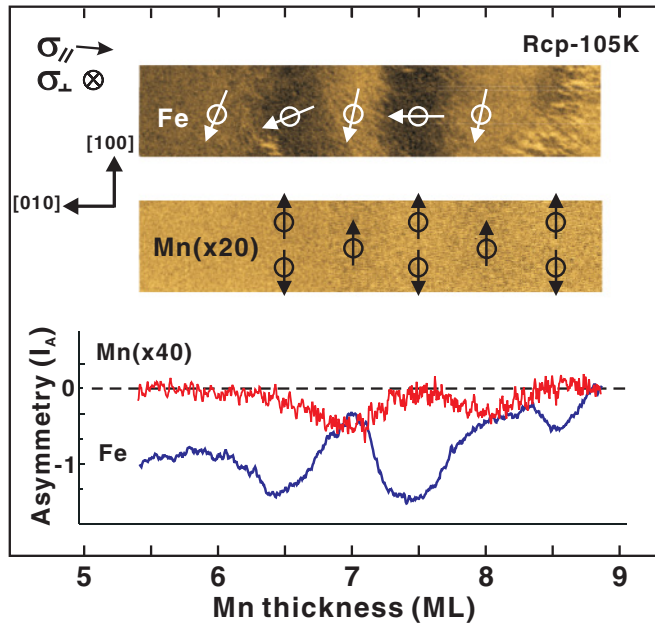


FIG. 5. (Color online) The Fe and Mn domain images as functions of t_{Mn} , taken at 105 K, at the region where the Fe film reveals the flipping magnetization (indicated by white arrows). The Mn layer yields nonvanishing I_A at integer layer thickness and approaches to zero value at half-integer layer thickness. A very small I_A signal for the Mn layer could be attributed to a nearly orthogonal included angle between the photohelicity and in-plane magnetization. The black arrows in the Mn image indicate the estimated arrangement of surface magnetization.

asymmetry arises for the Mn film with integer layer thickness, but an almost vanishing magnetic asymmetry occurs for the Mn film with half-integer layer thickness. The I_A curve of the Mn film not following exactly with the Fe curve indicates that the observed Mn magnetic asymmetry is not contributed by the induced moments of the Fe layer, but should be correlated with the surface spin arrangement originating from the intrinsic magnetic order of the Mn layer. In Fig. 5, although a variation of Mn magnetic asymmetry from zero to negative value might be contributed by the in-plane magnetization changing from the $[\pm 100]$ to $[0\bar{1}0]$ direction, from a symmetry consideration, a variation of Mn magnetization from $[\pm 100]$ to $[0\bar{1}0]$ leading to a positive value of I_A should also present at a certain thickness of Mn film. Thus, the absence of the positive feature in I_A of Fig. 5 suggests that the presence and vanishing of magnetic asymmetry with varying t_{Mn} should more likely correspond to the uncompensated and compensated magnetic surfaces of the Mn layer, respectively, parallel to $[\pm 100]$. The presence of magnetic asymmetry as $t_{Mn} > 6$ ML also indicates that the present condition of magnetic imaging is sufficient to sense the weak in-plane magnetization of the Mn layer. Therefore, the absent Mn magnetic asymmetry in the region of $t_{Mn} < 6$ ML could be attributed to the paramagnetic state of the Mn layer. The possible arrangements of Mn magnetic surfaces were estimated and plotted as the black arrows of Fig. 5, where the Fe-Mn magnetization could couple collinearly for Mn with integer layer thickness and at 90° for Mn with half-integer layer thickness. The modulation of interface exchange coupling between collinear and noncollinear configurations via varying

Mn thickness should be the origin of the observed 90° flipping magnetization of Fe film with the periodicity of 1 ML Mn thickness.

IV. DISCUSSION

The finding of 90° flipping magnetization of the Fe film and uncompensated-compensated transition of the Mn magnetic surface also provides a clue to differentiate the spin order of fcc-Mn between the two magnetic phases, an in-plane $c(2 \times 2)$ and the $[100]$ layered AFM proposed by Hafner and Spišák.²³ For in-plane $c(2 \times 2)$ spin order [Fig. 6(a)], the spins align collinearly and compensatively in the in-plane $[\pm 100]$ direction for each layer. If a noncollinear exchange coupling at the AFM-FM interface is established, the FM magnetization should keep an invariant direction while varying the AFM thickness. On the other hand, the layered AFM spin order [Fig. 6(b)] shows the spins fully align in the in-plane $[100]$ direction at the top layer, and reverse to the opposite direction at the second layer. The magnetic surface can be modulated from uncompensated to compensated due to the formation of monoatomic steps, if the film follows a layer-by-layer growth mode. This could result in the collinear and noncollinear Mn-Fe exchange coupling for Mn layers with integer and half-integer layer thickness, respectively, which causes the 90° flipping magnetization of the adjacent FM film with the variation of AFM film thickness. The latter case agrees well with the characteristics observed in the 8 ML

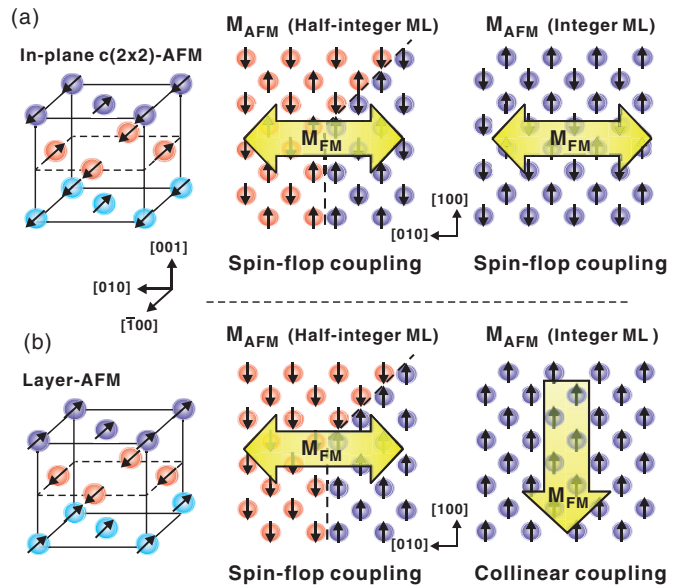


FIG. 6. (Color online) Two schematic models of AFM spin order predicted by *ab initio* calculation (Ref. 23). (a) In-plane $c(2 \times 2)$ spin order. The magnetic surface is compensated for the Mn layer with either half-integer or integer ML thickness. The FM spins are expected to be exchange coupled with both cases through 90° coupling. (b) Layered-AFM spin order. The magnetic surface is compensated for Mn with half-integer layer thickness, but uncompensated for that with integer layer thickness. The FM spins are expected to be exchange coupled with the former case through the 90° exchange coupling, but with the latter case through the collinear exchange coupling.

Fe/wedged-Mn bilayer, and therefore suggests a layered-like AFM configuration for the Mn layer.

V. SUMMARY

In summary, we have presented an element-resolved magnetic imaging investigation on a Fe/wedged-Mn bilayer. We demonstrate a 90° flipping magnetization of the FM layer, which is induced by a periodically modulated noncollinear-type exchange coupling between FM and AFM layers. Our work clarifies the interrelation between the magnetic reorien-

tation of a FM layer and interface exchange coupling with the adjacent AFM layer, and demonstrates an alternative way to explore the interface spin order of the antiferromagnet in an FM/AFM bilayer, which is still difficult to directly probe with conventional approaches.

ACKNOWLEDGMENT

This work was supported in part by the National Science Council of Taiwan through Grant No. NSC 99-2120-M-002-005.

*mtlin@phys.ntu.edu.tw

- ¹J. Nogués and I. K. Schuller, *J. Magn. Magn. Mater.* **192**, 203 (1999).
- ²J. C. S. Kools, *IEEE Trans. Magn.* **32**, 3165 (1996).
- ³S. D. Bader, *Rev. Mod. Phys.* **78**, 1 (2006).
- ⁴J. Stöhr and H. C. Siegmann, *Magnetism: From Fundamentals to Nanoscale Dynamics* (Springer, Berlin, 2006).
- ⁵C. L. Gao, A. Ernst, A. Winkelmann, J. Henk, W. Wulfhekel, P. Bruno, and J. Kirschner, *Phys. Rev. Lett.* **100**, 237203 (2008).
- ⁶U. Schlickum, N. Janke-Gilman, W. Wulfhekel, and J. Kirschner, *Phys. Rev. Lett.* **92**, 107203 (2004).
- ⁷J. C. Slonczewski, *Phys. Rev. Lett.* **67**, 3172 (1991).
- ⁸N. C. Koon, *Phys. Rev. Lett.* **78**, 4865 (1997).
- ⁹T. C. Schulthess and W. H. Butler, *Phys. Rev. Lett.* **81**, 4516 (1998).
- ¹⁰J. H. Seok, H. Y. Kwon, S. S. Hong, Y. Z. Wu, Z. Q. Qiu, and C. Won, *Phys. Rev. B* **80**, 174407 (2009).
- ¹¹S. H. Tsai, D. P. Landau, and T. C. Schulthess, *J. Appl. Phys.* **93**, 8612 (2003).
- ¹²T. J. Moran, J. Nogués, D. Lederman, and I. K. Schuller, *Appl. Phys. Lett.* **72**, 617 (1998).
- ¹³Y. Ijiri, J. A. Borchers, R. W. Erwin, S. H. Lee, P. J. van der Zaag, and R. M. Wolf, *Phys. Rev. Lett.* **80**, 608 (1998).
- ¹⁴Q. F. Zhan and K. M. Krishnan, *Appl. Phys. Lett.* **96**, 112506 (2010).
- ¹⁵J. T. Kohlhepp and W. J. M. de Jonge, *J. Appl. Phys.* **95**, 6840 (2004).
- ¹⁶H. Ohldag, A. Scholl, F. Nolting, S. Anders, F. U. Hillebrecht, and J. Stöhr, *Phys. Rev. Lett.* **86**, 2878 (2001).
- ¹⁷L. Duó, A. Brambilla, P. Biagioni, M. Finazzi, A. Scholl, G. H. Gweon, J. Graf, and A. Lanzara, *Surf. Sci.* **600**, 4160 (2006).
- ¹⁸J. Wu, J. Choi, A. Scholl, A. Doran, E. Arenholz, C. Hwang, and Z. Q. Qiu, *Phys. Rev. B* **79**, 212411 (2009).
- ¹⁹J. Fujii, F. Borgatti, G. Panaccione, M. Hochstrasser, F. Maccherozzi, G. Rossi, and G. van der Laan, *Phys. Rev. B* **73**, 214444 (2006).
- ²⁰W. Kuch, F. Offi, L. I. Chelaru, M. Kotsugi, K. Fukumoto, and J. Kirschner, *Phys. Rev. B* **65**, 140408 (2002).
- ²¹C. Won, Y. Z. Wu, H. W. Zhao, A. Scholl, A. Doran, W. Kim, T. L. Owens, X. F. Jin, and Z. Q. Qiu, *Phys. Rev. B* **71**, 024406 (2005).
- ²²G. Chen, J. Li, F. Z. Liu, J. Zhu, Y. He, J. Wu, Z. Q. Qiu, and Y. Z. Wu, *J. Appl. Phys.* **108**, 073905 (2010).
- ²³J. Hafner and D. Spišák, *Phys. Rev. B* **72**, 144420 (2005).
- ²⁴Martin Zelený, F. D. Natterer, A. Biedermann, and J. Hafner, *Phys. Rev. B* **82**, 165422 (2010).
- ²⁵J. Stöhr, Y. Wu, B. D. Hermsmeier, M. G. Samant, G. R. Harp, S. Koranda, D. Dunham, and B. P. Tonner, *Science* **259**, 658 (1993).
- ²⁶C. M. Schneider and G. Schönhense, *Rep. Prog. Phys.* **65**, R1785 (2002).
- ²⁷W. C. Lin, T. Y. Chen, L. C. Lin, B. Y. Wang, Y. W. Liao, K. J. Song, and M. T. Lin, *Phys. Rev. B* **75**, 054419 (2007).
- ²⁸B. Y. Wang, N. Y. Jih, W. C. Lin, C. H. Chuang, P. J. Hsu, C. W. Peng, Y. C. Yeh, Y. L. Chan, D. H. Wei, W. C. Chiang, and M. T. Lin, *Phys. Rev. B* **83**, 104417 (2011).
- ²⁹C. L. Gao, A. Ernst, G. Fischer, W. Hergert, P. Bruno, W. Wulfhekel, and J. Kirschner, *Phys. Rev. Lett.* **101**, 167201 (2008).
- ³⁰B. Schirmer, B. Feldmann, A. Sokoll, Y. Gauthier, and M. Wuttig, *Phys. Rev. B* **60**, 5895 (1999).
- ³¹A. C. Lawson, A. C. Larson, M. C. Aronson, Z. Fisk, P. C. Canfield, J. D. Thompson, R. B. von Dreele, and S. Johnson, *J. Appl. Phys.* **76**, 7049 (1994).
- ³²M. ÓKeefe and S. Andersson, *Acta Crystallogr. Sect. A* **33**, 914 (1977).
- ³³J. T. Kohlhepp and W. J. M. de Jonge, *Phys. Rev. Lett.* **96**, 237201 (2006).
- ³⁴J. T. Kohlhepp, H. Wieldraaijer, and W. J. M. de Jonge, *Appl. Phys. Lett.* **89**, 032507 (2006).
- ³⁵T. Oguchi and A. J. Freeman, *J. Magn. Magn. Mater.* **46**, L1 (1984).
- ³⁶Yasuo Endoh and Yoshikazu Ishikawa, *J. Phys. Soc. Jpn.* **30**, 1614 (1971).
- ³⁷M. T. Lin, J. Shen, W. Kuch, H. Jenniches, M. Klaua, C. M. Schneider, and J. Kirschner, *Phys. Rev. B* **55**, 5886 (1997).
- ³⁸F. Bisio, S. Terreni, M. Canepa, and L. Mattera, *Phys. Rev. B* **72**, 174413 (2005).
- ³⁹T. Ambrose and C. L. Chien, *Phys. Rev. Lett.* **76**, 1743 (1996).
- ⁴⁰S. K. Mishra, F. Radu, S. Valencia, D. Schmitz, E. Schierle, H. A. Dürr, and W. Eberhardt, *Phys. Rev. B* **81**, 212404 (2010).